Correlation Function Quantum Monte Carlo Study of the Excited Vibrational States of $H_5O_2^+$ †

Hyung Min Cho and Sherwin J. Singer*

Department of Chemistry, The Ohio State University, 100 W. 18th Avenue, Columbus, Ohio 43210

Received: April 9, 2004; In Final Form: June 12, 2004

Full dimensional (15 df) quantum Monte Carlo calculations of vibrational energies of $H_5O_2^+$ are reported using the OSS3(p) potential energy surface of Ojamäe et al. [Ojamäe, L.; Shavitt, I.; Singer, S. J. *J. Chem. Phys.* **1998**, *109*, 5547]. The protonated water dimer, $H_5O_2^+$, is an important case for vibrational study for the purpose of understanding the potential energy surface of the smallest aqueous proton-transfer system. Vibrational calculations are quite difficult for this system because of its high dimensionality and strong coupling between anharmonic low-frequency coordinates, among them motion of the central proton, which is associated with the most intense vibrational modes. In our study, the correlation function quantum Monte Carlo (CFQMC) method is employed for a full-dimensional treatment of the system. The development of an improved trial wave function gave a better starting point for understanding the excited states and was a crucial step that enabled us to obtain a set of converged energy eigenvalues using the CFQMC method. Several methods of extrapolating energy eigenvalues from the CFQMC data were evaluated. Transition moments were calculated to help identification of the excited states and allowed us to obtain exact information about most of the fundamental frequencies of the $H_5O_2^+$ ion.

1. Introduction

Water is one of the most abundant substances of the earth's crust. All of chemical reactions occurring in living organisms take place in an aqueous environment. Water has unusual physiochemical properties and plays a central role in many key industrial and biological reactions as well. Thus, it is no wonder that water has been a focus of experimental and theoretical research for a long period of time. One of the well-known fundamental properties of water is its extremely high proton mobility, which cannot be understood as an ordinary diffusion process. Proton transport in water is best pictured as a sequence of proton-transfer events between water molecules that belong to a hydrogen bond network. Because of the importance of proton-transfer processes in many biological systems and for other types of aqueous chemistry, extensive theoretical and experimental efforts have been devoted to understanding similar phenomena in small water clusters.

As the smallest purely aqueous proton-transfer system, $H_5O_2^+$ has been studied for more than 30 years.[1−49] Despite the small size of this species, characterization of the vibrational excited states of $H_5O_2^+$ has been a major challenge. A proton is equally shared by two water molecules in the ground state. However, the potential energy surface along the central proton coordinate is so flat that the motion of the central proton exhibits large amplitude motion even in the ground state, as shown in our previous study of the ground vibrational state.[48] Such large amplitude motion naturally incurs change in character from the symmetric nonclassical ion to an H_3O^+/H_2O pair when the central proton departs from its equilibrium. Bond lengths and bond angles change between those characteristic of water to those characteristic of hydronium as the central proton oscillates between the two oxygens. Therefore, considerable anharmonic coupling arises between many vibrational modes and low-frequency modes involving central proton motion. The result is a very complicated vibrational structure that makes normal-mode analysis based on the harmonic approximation almost meaningless, especially for the description of the proton-transfer mode. Because of the high dimensionality of $H_5O_2^+$, traditional variational methods based on a basis set expansion have limited applicability.

Experimental vibrational data for $H_5O_2^+$ had been quite limited except for the terminal OH stretching modes.[39,40] The most important modes yet to be resolved are those involving the central proton-transfer coordinate. Very recently, a low resolution infrared spectrum of $H_5O_2^+$ in the gas phase was reported that covered the central proton-transfer region.[42] However, fundamental frequencies were not identified from among the various bands in this low resolution of this experiment and the assignment of observed spectral lines are still in debate.[37,42,47,49]

There have been several previous attempts to theoretically calculate the vibrational spectrum of $H_5O_2^+$. Harmonic frequencies have been reported in conjunction with ab initio studies of the equilibrium geometry and potential surface.[6,9,12,16,17,19,26,36−38] Anharmonic effects have been estimated using molecular dynamics simulations.[43−46,50,51] Chaban et al.[47] reported vibrational self-consistent field calculations for $H_5O_2^+$ corrected with perturbation theory. They used a two-mode representation of the potential surface, which may be inadequate because many coordinates in $H_5O_2^+$ are strongly coupled. Vener et al.[36,37] devised reduced three- and four-dimensional models for $H_5O_2^+$, taking the coordinates of the central proton and oxygen−oxygen stretch as active while fixing the remaining coordinates at their minimum energy values as functions of the active coordinates.

Two studies using the OSS3(p) surface have recently appeared.[48,49] First, in conjunction with our QMC study of the ground vibrational state, the Bowman group performed MULTIMODE calculations to obtain the vibrational zero-point energy and fundamental frequencies. Second, Dai et al. performed

† Part of the "Gert D. Billing Memorial Issue".

* To whom correspondence should be addressed. E-mail: singer@chemistry.ohio-state.edu.

10.1021/jp0484175 CCC: $27.50
Published on Web 08/18/2004

approximate and exact calculations for reduced dimensional models similar to those of Vener et al., but based on the OSS3-(p) surface, and compared them to full-dimensional MULTIMODE results. Dai et al. criticized the way in which Vener et al. solved their reduced dimensional model, showing that those previous approximations led to considerable error. They also demonstrated that the reduced dimensional model was of limited value for important modes such as the proton-transfer motion. The MULTIMODE calculations were based on a four-mode representation of the potential surface. While perhaps the most extensive treatment of the vibrations of $H_5O_2^+$ to date, the MULTIMODE results are approximate due to the representation of the potential and truncation of the basis. The ground-state energy estimated in the MULTIMODE calculations is 101 cm^{-1} higher than the true ZPE for the OSS3(p) surface obtained from our QMC calculations. The ZPE obtained from our QMC calculations is the result of a careful extrapolation with respect to the imaginary time step and is estimated to be within 1 cm^{-1} of the exact result.[48] A rough estimate of the error in the MULTIMODE fundamental frequencies is provided by assuming harmonic behavior, where the fundamental frequency is twice the zero-point energy for each mode. The 101 cm^{-1} error in the ZPE would then translate into a net (summed over all modes) ~200 cm^{-1} error in the fundamental frequencies. The $H_5O_2^+$ ion is highly anharmonic, so this estimate is only a rough guide. Part of the motivation for the current work is to help identify the modes which might be in error and to provide benchmarks, within the limits of excited-state QMC methods (as discussed in section 5.3), for future calculations.

In this report, we present our recent full-dimensional excited state study of $H_5O_2^+$ using correlation function quantum Monte Carlo (CFQMC) method with the potential energy surface OSS3(p) that was used in the ground state study of $H_5O_2^+$. The CFQMC is briefly reviewed in section 2. Construction of trial excited-state basis functions is described in section 3. Technical details of the simulations are given in section 4. In section 5, we present results for ground and excited vibrational states of $H_5O_2^+$. Our conclusions are summarized in the final section.

2. Correlation Function Quantum Monte Carlo

The CFQMC method[52] is essentially a traditional variational calculation method augmented by basis relaxation and Monte Carlo sampling for multidimensional integrals. The CFQMC method has attracted recent attention[53−62] because it makes high-dimensionality problems tractable within the framework of traditional variational treatment.

Relaxed basis functions $\{\tilde{f}_i\}$ are generated from an initial set $\{f_i\}$ by application of the imaginary time propagator,

$$\tilde{f}_i = e^{-tH/2} f_i \tag{1}$$

where H is the full Hamiltonian operator and t is the (imaginary) time. The resulting generalized eigenvalue equation is

$$\mathbf{H}(t)C_j(t) = \lambda_j(t)\mathbf{N}(t)C_j(t) \tag{2}$$

where $\mathbf{H}(t)$ and $\mathbf{N}(t)$, to be evaluated using quantum Monte Carlo (QMC) techniques, are given by

$$H_{ij}(t) = \langle f_i | e^{-tH/2} H e^{-tH/2} | f_j \rangle = \int d\mathbf{R_1} d\mathbf{R_2} f_i(\mathbf{R_2}) \langle \mathbf{R_2} | H e^{-tH} | \mathbf{R_1} \rangle f_j(\mathbf{R_1}) \tag{3}$$

$$N_{ij}(t) = \langle e^{-tH/2} f_i | e^{-tH/2} f_j \rangle = \int d\mathbf{R_1} d\mathbf{R_2} f_i(\mathbf{R_2}) \langle \mathbf{R_2} | e^{-tH} | \mathbf{R_1} \rangle f_j(\mathbf{R_1}) \tag{4}$$

assuming a real primitive basis set $\{f_i\}$. At the projection time $t = 0$, the CFQMC reduces to a conventional variational Monte Carlo estimate of the ground and excited eigenvalues. The ith eigenvalue $\lambda_i(t)$, for the moment not considering statistical error, is an upper bound to the true energy eigenvalue E_i and converges exponentially to E_i as the projection time grows:

$$\lim_{t\to\infty} \lambda_i(t) = E_i \tag{5}$$

As proposed by Ceperley and Bernu, the matrix elements in eqs 3 and 4 can be cast in a form suitable for QMC evaluation using a guiding function $\psi(\mathbf{R})$.

$$H_{ij}(t) = \int d\mathbf{R_1} d\mathbf{R_2} F_i(\mathbf{R_2}) E_{Li}(\mathbf{R_2}) G(\mathbf{R_2},\mathbf{R_1};t) F_j(\mathbf{R_1}) P(\mathbf{R_1}) \tag{6}$$

$$N_{ij}(t) = \int d\mathbf{R_1} d\mathbf{R_2} F_i(\mathbf{R_2}) G(\mathbf{R_2},\mathbf{R_1};t) F_j(\mathbf{R_1}) P(\mathbf{R_1}) \tag{7}$$

In the equation above, $F_i(\mathbf{R})$ and $P(\mathbf{R})$ are

$$F_i(\mathbf{R}) = \frac{f_i(\mathbf{R})}{\psi(\mathbf{R})} \tag{8}$$

and

$$P(\mathbf{R}) = \psi^2(\mathbf{R}) \tag{9}$$

respectively.

$E_{Li}(\boldsymbol{R})$ is the local energy of the primitive basis function f_i, which is defined as

$$E_{Li}(\mathbf{R}) = \frac{H f_i(\mathbf{R})}{f_i(\mathbf{R})} \tag{10}$$

Note that $E_{Li}(\mathbf{R})$ is different from the local energy of the guiding function $E_{L\psi}(\mathbf{R})$.

The matrix elements $H_{ij}(t)$ and $N_{ij}(t)$ can be estimated as averages over points $\mathbf{R}_n$ sampled from a random walk governed by the pure diffusion short time Green's function.

$$G_{\mathrm{diff}}(\mathbf{R}_{n+1},\mathbf{R}_n;\tau) = \prod_{i=1}^{n_D} \left(\frac{1}{4D_i\pi\tau}\right)^{3/2} \exp\left[\frac{-(\mathbf{R}^i_{n+1} - \mathbf{R}^i_n - D_i\tau F^i(\mathbf{R}_n))^2}{4D_i\tau}\right] \tag{11}$$

where the index i runs over the n_D dimensions of the system, $D_i \equiv \hbar^2/2m_i$, τ is the time step, and $F^i(\mathbf{R})$ is the quantum force defined as

$$F^i(\mathbf{R}) = \frac{2}{\psi(\boldsymbol{R})} \nabla_i \psi(\mathbf{R}) \tag{12}$$

In terms of elements from random walk of length p,

$$N_{ij}(k\tau) = \left\langle \frac{1}{(p-k)} \sum_{n=1}^{p-k} F_i(\mathbf{R}_n) W_{n,n+k} F_j(\mathbf{R}_{n+k}) \right\rangle \tag{13}$$

$$H_{ij}(k\tau) = \left\langle \frac{1}{(p-k)} \sum_{n=1}^{p-k} F_i(\mathbf{R}_n) W_{n,n+k} F_j(\mathbf{R}_{n+k}) E_{Lj}(\mathbf{R}_{n+k}) \right\rangle \quad (14)$$

where the angle brackets denote averaging over multiple walkers and the weight is defined as

$$W_{n,n+k} = \exp\left\{ -\frac{\tau}{2} \sum_{l=n}^{n+k-1} [E_{L\psi}(\mathbf{R}_l) + E_{L\psi}(\mathbf{R}_{l+1})] \right\} \quad (15)$$

Finally, the matrixes are symmetrized in practice to reduce the statistical noise.

Because the length of the random walk cannot be made infinitely long in practice, the estimated matrix elements are subject to statistical errors. Ceperley and Burnu presented a detailed analysis on the errors involved in the CFQMC procedure.[52] One of the major consequences of the error analysis is that the error grows exponentially with the projection time and the excitation energy. Thus, the CFQMC method is best suited to computation of low-lying excited quantum states in general.

There are several other schemes for calculation of excited states using QMC methods. (See refs 52 and 63 for surveys of excited state QMC methods.) Eigenvalues can be extracted by inverse Laplace transformation of an imaginary time correlation function.[64−66] In general, a single correlation function would not contain enough information to obtain many fundamental frequencies, especially for a system as large as $H_5O_2^+$. However, projection operator methods can enhance the efficiency of inverse Laplace transform methods.[67−71] Excited-state energies can be estimated by introducing a node in the wave function.[72−75] This method can be extended by optimizing the nodal surface.[66,76−79] The optimized node method has been applied to rather large sytems in the context of rigid-body diffusion Monte Carlo.[80] The very floppy nature and strong coupling of all degrees of freedom in $H_5O_2^+$ precludes the use of a rigid-body approximation for this system. Fixed or optimized node methods work best when one has some guidance where the node should appear, either from symmetry or a good zero-order model. Such methods might have applicability to a system like $H_5O_2^+$, especially if one focused on a particular excited level. In this work we attempt to calculate a broad selection of fundamental frequencies of $H_5O_2^+$, and CFQMC appears most appropriate for this task. The review by Prudent et al.[63] describes several cases where CFQMC methods have been used to obtain accurate rovibrational eigenvalues.

3. Trial Excited Basis Functions

3.1. General Aspects and Considerations. In the CFQMC method, the quality of the initial basis functions $\{f_i\}$ is crucial for obtaining useful information before statistical error overwhelms the calculation at long projection time.

Although there have been some suggestions in the literature as to the form of trial basis functions for rovibrational problems,[53,54,63,81,82] how to choose a simple, yet good quality trial basis set is still an open question. In our calculation, we employed trial basis functions in the form proposed by Acioli and Soares Neto.[53] This is a slightly modified version from what Bernu et al. suggested originally[81] and has been successfully used for the vibrational study of small molecules.[53] We devised coordinates that were suited for the description of some low-energy states which arise from the floppy motion of water monomers within $H_5O_2^+$.

Acioli and Soares Neto suggested a basis set of the form

$$f_i = \psi_{\text{trial}} \left(\prod_{\nu=1}^{N_p} \Delta S_\nu^{n_\nu(i)} \right) \quad (16)$$

where ψ_{trial} is an approximation to the ground-state wave function, $\{\Delta S_\nu\}$ are local modes defined as change in interatomic distances from those at the equilibrium, and $\{n_\nu(i)\}$ is a set of integers assigned to local modes in basis function i.

This form of excited basis set has been tested in vibrational studies of small molecules up to tetra-atomic molecules and has proven to be effective.[53] There have been more complex forms of basis sets proposed by other authors[54,82] based on Morse oscillator eigenfunctions.[83]

While previous works used a Gaussian *ansatz* for ψ_{trial}, we found that better approximations were rewarded with significantly reduced statistical error. Our trial wave function is expressed in terms of the internal coordinates specified in Table 1 with the labeling scheme illustrated in Figure 1.

The trial wave function is of the form

$$\psi_{\text{trial}} \propto \mathrm{e}^{-f} \quad (17)$$

where

$$f = v_1(d_a) + v_1(d_b) + v_2(R) + v_3(z) + \sum_{i=1}^{4} v_4(d_{\mathrm{OH}_i}) + v_5(d_{\mathrm{HH}_a}) + v_5(d_{\mathrm{HH}_b}) + v_6(w_a) + v_6(w_b) + v_7(\theta_{ab}) + v_8(\theta_a) + v_8(\theta_b) + \sum_{i=1}^{4} v_9(d_i) + v_{10}(|\mathbf{r}_B - \mathbf{r}_3|) + v_{10}(|\mathbf{r}_C - \mathbf{r}_3|) + \text{coupling terms} \quad (18)$$

the coupling terms are specified in Table 2, and

$$d_i = |\mathbf{r}_{i+3} - \mathbf{r}_3|$$

(distances between central and outer hydrogens)

$$i = 1, 2, 3, 4$$

$$v_j(x_\mu) = \frac{1}{2} K_j^2 (x_\mu - x_{\mu j}^0)^2 \qquad j > 2$$

$$v_j(x_\mu) = \frac{1}{2} K_j (x_\mu - x_{\mu j}^0)^2 + \frac{1}{3} L_j (x_\mu - x_{\mu j}^0)^3 + \frac{1}{4} M_j^2 (x_\mu - x_{\mu j}^0)^4 \qquad j \le 2 \quad (19)$$

A trial wave function with 36 parameters was optimized by minimizing the energy in variational Monte Carlo (VMC) calculations.

We employed both distances and angles in the construction of excited basis functions instead of local modes as in eq 16. The general form of our excited-state basis is

$$f_i = \psi_{\text{trial}} \left(\prod_{\nu=1}^{N_p} \Delta g_\nu^{n_\nu(i)} \right) \quad (20)$$

where ψ_{trial} is the trial guiding function used in the ground state study, N_p is the number of modes included to construct given basis functions, and the $\{n_\nu(i)\}$ is a set of integers assigned to the coordinates involved in basis function i. g_ν is similar to the local mode in eq 16 but is not limited to distances. Instead, g_ν can be distances, angles, or any coordinates which are designed to represent specific modes. For the description of central proton motion and oxygen−oxygen stretching, g_ν is an interatomic

TABLE 1: Coordinates Used for $H_5O_2^+$ Trial Guiding Function[a]

coordinate	definition	characterization
d_a	$\|\mathbf{r}_2 - \mathbf{r}_3\|$	inner proton to oxygen stretch
d_b	$\|\mathbf{r}_1 - \mathbf{r}_3\|$	inner proton to oxygen stretch
R	$\|\mathbf{r}_1 - \mathbf{r}_2\|$	oxygen−oxygen distance
z	$\|\mathbf{r}_3 - \mathbf{r}_A\|$	deviation of inner proton from oxygen−oxygen axis
d_{OH_1}	$\|\mathbf{r}_1 - \mathbf{r}_4\|$	outer oxygen−hydrogen stretch
d_{OH_2}	$\|\mathbf{r}_1 - \mathbf{r}_6\|$	outer oxygen−hydrogen stretch
d_{OH_3}	$\|\mathbf{r}_2 - \mathbf{r}_5\|$	outer oxygen−hydrogen stretch
d_{OH_4}	$\|\mathbf{r}_2 - \mathbf{r}_7\|$	outer oxygen−hydrogen stretch
d_{HH_a}	$\|\mathbf{r}_4 - \mathbf{r}_6\|$	outer hydrogen−hydrogen distance, a water bend coordinate
d_{HH_b}	$\|\mathbf{r}_5 - \mathbf{r}_7\|$	outer hydrogen−hydrogen distance, a water bend coordinate
w_a	$(\mathbf{r}_B - \mathbf{r}_1)\cdot(\mathbf{r}_1 - \mathbf{r}_2)$	water molecule wag
w_b	$(\mathbf{r}_C - \mathbf{r}_2)\cdot(\mathbf{r}_2 - \mathbf{r}_1)$	water molecule wag
θ_{ab}	$\{[(\mathbf{r}_4 - \mathbf{r}_6)\cdot(\mathbf{r}_5 - \mathbf{r}_7)]/[\|\mathbf{r}_4 - \mathbf{r}_6\|\|\mathbf{r}_5 - \mathbf{r}_7\|]\}^2$	torsional coordinate measuring alignment of outer waters
θ_a	$\{[(\mathbf{r}_4 - \mathbf{r}_6)\cdot(\mathbf{r}_3 - \mathbf{r}_A)]/\|\mathbf{r}_4 - \mathbf{r}_6\|\}^2$	torsional coordinate measuring alignment of waters with the direction by which the central proton deviates from the oxygen−oxygen bond
θ_b	$\{[(\mathbf{r}_5 - \mathbf{r}_7)\cdot(\mathbf{r}_3 - \mathbf{r}_A)]/\|\mathbf{r}_5 - \mathbf{r}_7\|\}^2$	torsional coordinate measuring alignment of waters with the direction by which the central proton deviates from the oxygen−oxygen bond

[a] Definitions make use of several intermediate points: the midpoint of oxygen−oxygen bond, $\mathbf{r}_A \equiv {}^1/_2(\mathbf{r}_1 + \mathbf{r}_2)$, and the two midpoints between outer hydrogen pairs, $\mathbf{r}_B \equiv {}^1/_2(\mathbf{r}_4 + \mathbf{r}_6)$ and $\mathbf{r}_C \equiv {}^1/_2(\mathbf{r}_5 + \mathbf{r}_7)$.

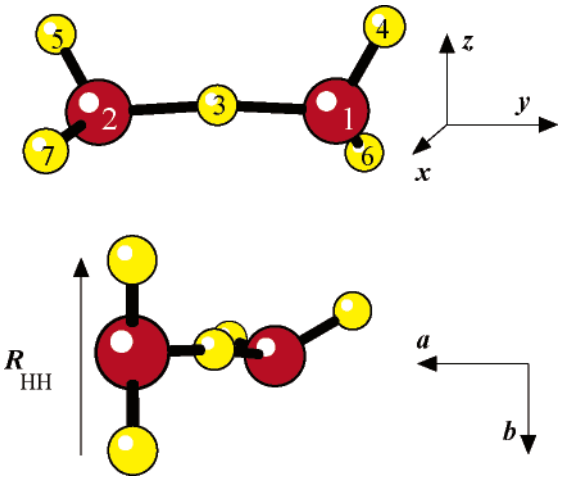

Figure 1. Top view: $H_5O_2^+$ in its equilibrium geometry, indicating the labeling of the atoms used in Table 1. Bottom view: $H_5O_2^+$ drawn to illustrate an axis system for the torsion coordinates of the terminal water molecule. The molecular bisector vector points outward from the oxygen atom perpendicular to the plane of the page.

distance. To represent the complex torsional motion of water monomers within $H_5O_2^+$, new coordinates are defined.

3.2. Coordinates for Central Proton and Torsional Motion. A molecule fixed coordinate system is set within $H_5O_2^+$ with the oxygen−oxygen axis taken as the *y* direction. The *z*-axis is perpendicular to *y* and points toward the position of the central proton. The *x*-axis is naturally chosen mutually perpendicular to *y* and *z* and forms a right-handed coordinate system. Then, we define a vector which represents deviation of the central proton from the midpoint of the oxygen−oxygen axis as

$$\mathbf{r} = \mathbf{r}_3 - \mathbf{r}_A \tag{21}$$

where $\mathbf{r}_3$ is the coordinate vector of the central proton and $\mathbf{r}_A$ is the average of the two oxygen positions. By definition, the *x*-component of $\mathbf{r}$ is always zero. The direction of the rotation axis of the outer water monomers is specified by the instantaneous molecular bisector, $\mathbf{B}_i$, $i = 1, 2$. Description of the orientation of two outer hydrogen atoms about this bisector needs another reference direction perpendicular to it. As shown in Figure 1, a vector $\mathbf{a}_i$, the component of the oxygen−oxygen vector $\mathbf{R}_{oo}$ perpendicular to the bisector, can provide this reference,

$$\mathbf{a}_i = \mathbf{R}_{oo} - (\mathbf{R}_{oo}\cdot\hat{\mathbf{B}}_i)\hat{\mathbf{B}}_i, \qquad i = 1, 2 \tag{22}$$

Finally, a third vector, $\mathbf{b}_i$, completes a right-handed coordinate system.

$$\mathbf{b}_i = \hat{\mathbf{B}}_i \times \mathbf{a}_i, \qquad i = 1, 2 \tag{23}$$

The **a**−**b** coordinate system for each water molecule provides a way to specify the torsion coordinate and fully determine the orientation of the water units. We employed the components of the hydrogen−hydrogen vectors $\mathbf{R}_{HH,i}$ along the **a** and **b** axes as torsional coordinates.

$$u_{a,i} = \mathbf{R}_{HH,i}\cdot\mathbf{a}_i \tag{24}$$

$$u_{b,i} = \mathbf{R}_{HH,i}\cdot\mathbf{b}_i \tag{25}$$

Multiplying the trial ground-state wave function by $u_{a,i}$ places a node at the equilibrium torsion angle and thereby generates an initial approximation to a torsionally excited basis (before combining $u_{a,1}$ and $u_{a,2}$ to form symmetry-adapted combinations). Alternatively, multiplying by $u_{b,i}$ places a node near the transition state for internal rotation of a water unit about the bisector, the motion that leads to exchange of the two hydrogens of the outer water unit.

Another torsional coordinate is generated by the projections of the bisectors on the **x** and **z** axis defined by the central proton.

$$t_{x,i} = \mathbf{B}_i\cdot\mathbf{x} \tag{26}$$

$$t_{z,i} = \mathbf{B}_i\cdot\mathbf{z} \tag{27}$$

In the above equation, **x** and **z** are components of the vector **r** defined in eq 21. We prefer to project onto **x** and **z**, and not unit vectors in those directions, to avoid singularities which arise when the central proton passes near the oxygen−oxygen axis. (The same consideration led us to not take $\mathbf{a}_i$ and $\mathbf{b}_i$ in eq 22 and eq 23 as unit vectors.) The two sets of torsion coordinates, $(u_{a,i}, u_{b,i})$ and $(t_{x,i}, t_{z,i})$, transform differently under permutation-inversion group operations, as discussed in section 3.3. At the equilibrium position, neither $t_{x,i}$ nor $t_{z,i}$ are zero.

TABLE 2: Coupling Terms Used for $H_5O_2^+$ Guiding Function[a]

term	characterization
$\alpha_1[(d_{OH_1}-\alpha_2)(d_{HH_a}-\alpha_3)+(d_{OH_2}-\alpha_2)(d_{HH_a}-\alpha_3)$ $+(d_{OH_3}-\alpha_2)(d_{HH_b}-\alpha_3)+(d_{OH_4}-\alpha_2)(d_{HH_b}-\alpha_3)]$	OH−HH coupling
$\alpha_4(d_a+d_b-2\alpha_{16})(R-\alpha_5)$	*R*, central proton stretch coupling
$\alpha_6[(d_a-\alpha_{16})(d_{HH_a}-\alpha_3)+(d_b-\alpha_{16})(d_{HH_b}-\alpha_3)]$ $+\alpha_7[(d_b-\alpha_{16})(d_{HH_a}-\alpha_3)+(d_a-\alpha_{16})(d_{HH_b}-\alpha_3)]$	water HH, central proton stretch coupling
$\alpha_9(R-\alpha_5)(d_{OH_1}+d_{OH_2}+d_{OH_3}+d_{OH_4}-4\alpha_2)$	*R*, OH coupling
$\alpha_{10}(R-\alpha_5)(w_a+w_b-2\alpha_8)$	water wag, R coupling
$\alpha_{11}[(d_1-\alpha_{12})(d_3-\alpha_{12})+(d_2-\alpha_{12})(d_4-\alpha_{12})]$	hydronium bending coupling
$(d_{OH_1}-\alpha_{13})[\alpha_{14}(d_1-\alpha_{12})+\alpha_{15}(d_3-\alpha_{12})]$ $+(d_{OH_2}-\alpha_{13})[\alpha_{15}(d_1-\alpha_{12})+\alpha_{14}(d_3-\alpha_{12})]$ $+(d_{OH_3}-\alpha_{13})[\alpha_{14}(d_2-\alpha_{12})+\alpha_{15}(d_4-\alpha_{12})]$ $+(d_{OH_4}-\alpha_{13})[\alpha_{15}(d_4-\alpha_{12})+\alpha_{14}(d_2-\alpha_{12})]$	OH, hydronium bending coupling
$(d_a-\alpha_{16})(d_1+d_3-2\alpha_{12})+(d_b-\alpha_{16})(d_2+d_4-2\alpha_{12})$	central proton stretch, hydrogen bending coupling
$\alpha_{17}[(d_a-\alpha_{16})(w_a-\alpha_8)+(d_b-\alpha_{16})(w_b-\alpha_8)]+$ $\alpha_{18}[(d_b-\alpha_{16})(w_a-\alpha_8)+(d_a-\alpha_{16})(w_b-\alpha_8)]$	wag, central proton stretch coupling

[a] $\{\alpha_k\}$ are parameters of the guiding function which were optimized in a variational Monte Carlo calculation prior to the CFQMC calculation.

TABLE 3: Symmetry-Adapted g_ν Factors Used To Construct Excited Basis Functions for $H_5O_2^+$

A_1^+	B_1^+	E^+
d_a+d_b	d_a+d_b	$u_{a,1}$, $u_{a,2}$
$d_{OH_1}+d_{OH_2}+d_{OH_3}+d_{OH_4}$	$d_{OH_1}+d_{OH_2}-d_{OH_3}-d_{OH_4}$	$d_{OH_1}-d_{OH_2}$, $d_{OH_3}-d_{OH_4}$
$d_1+d_2+d_3+d_4$	$d_1+d_3-d_2-d_4$	d_1-d_3, d_2-d_4
$d_{HH_a}+d_{HH_b}$	$d_{HH_a}-d_{HH_b}$	
w_a+w_b	w_a-w_b	
$t_{z,1}+t_{z,2}$	$t_{z,1}-t_{z,2}$	
$(t_{x,1})^2+(t_{x,2})^2$	$(t_{x,1})^2-(t_{x,2})^2$	
R		
θ_{ab}		
$t_{z,1}t_{z,2}$		
$t_{x,1}t_{x,2}$		
$(u_{a,1}u_{a,2})^2$		

3.3. The Symmetry of Basis Functions. The barrier for hindered rotational motion of the two water monomers about their bisectors is the lowest among the internal rearrangement pathways of $H_5O_2^+$.[15] In our QMC sampling, exchange of the two hydrogens of the outer water units occurred frequently, and all permutational isomers of this type were equally represented in our sampled populations.[48] The point symmetry group analysis of molecular vibrations for $H_5O_2^+$ is based on a rigid model which does not allow the hindered rotational motion of the outer water units. To take this nonrigid character into account, the nuclear permutation inversion (PI) group representation is adopted in our study. The choice of PI group is determined by the set of exchange of pathways which are significant, i.e., by the barrier heights, which is reflected in the selection of a group of permutations deemed to be "feasible". The barrier for exchange of the central hydrogen with hydrogens of the water monomers is considerably higher, and this motion is not considered as feasible in the present study. The PI group excluding this central proton exchange is G_{16}, which is isomorphic to that of the neutral water dimer.

Symmetry-adapted g_ν factors were constructed from the distances and angles introduced in the previous section. As a result, the Hamiltonian separates into A_1^+, B_1^+, and E^+ blocks. In principle, we could have constructed basis functions belonging to other representations of G_{16} using g_ν factors of the appropriate symmetry. These states would complete the tunneling multiplets of $H_5O_2^+$. However, calculation of tunneling splitting is beyond the scope of this work. The symmetry-adapted g_ν factors we used to construct trial excited vibrational states are given in Table 3. The g_ν factors are defined in terms of coordinates specified in Table 1 or the torsional coordinates discussed in section 3.2. Many of the choices in Table 3 are obvious, but some require some explanation. $H_5O_2^+$ can exist in two nonsuperimposable isomers related by a mirror reflection. The torsion coordinate $t_{z,i}$ is unchanged by this operation, but $t_{x,i}$ changes sign. To work with the same g_ν factors for both isomers of $H_5O_2^+$, we used $(t_{x,i})^2$ instead of $t_{x,i}$. This did not change the nature of the excited states from a fundamental to an overtone because $t_{x,i}$ is nonzero in the equilibrium geometry of $H_5O_2^+$. Analysis of the zero-point fluctuations of $H_5O_2^+$ (see Figure 6 of ref 48) reveals significant correlation between the hindered rotational motion of the two outer water molecules. Accordingly, we included several product terms among the excited-state basis involving torsional coordinates.

The number of coordinates of E^+ symmetry we constructed is relatively small. Consequently, our results for the E^+ block are of lower quality than the A_1^+ or B_1^+ blocks. We were only successful in calculating the eigenenergies of one low-lying E^+ state. Pinning down more excited E^+ states would require more coordinates of E^+ symmetry and inclusion of many g_ν factors built from direct products of coordinates with either A_1^+ or B_1^+ symmetry with E^+ coordinates.

4. Details of Simulation

4.1. The Guiding Function. In practice, almost all of the CFQMC calculations reported to date have used rather a simple form of guiding function proposed by Bernu et al.,[81] which is

$$\Psi = (\psi_{\text{trial}})^\gamma \tag{28}$$

where ψ_{trial} is the ground-state guiding function and γ is a parameter chosen to reduce the statistical fluctuations of the Hamiltonian matrix. In this study, we found optimum performance with $\gamma = 0.8$ and used this value throughout all the calculations reported in here.

4.2. Automated Code Generation. Because of the "anharmonic" terms in our ψ_{trial} [compare eqs 17−19 to the usual Gaussian *ansatz*] and the flexible form of our g_ν factors, implementation of ψ_{trial}, $E_{Li}(\mathbf{R})$, and $E_{L\psi}(\mathbf{R})$ in a computer program is a complex task. This difficulty was alleviated by using the symbolic algebra program[84] to assemble all the necessary derivatives and to generate the required FORTRAN code. The exponent f for ψ_{trial} and g_ν factors were input as algebraic expressions. In total, roughly 15000 lines of FORTRAN code were output from the symbolic algebra program and imported to the appropriate subroutines.

4.3. Identification of States and Transition Moments Calculation. Whether by direct diagonalization or via QMC methods, assignment of vibrational states is often troublesome using exact numerical methods. Sometimes the true eigenstates involve so many coupled coordinates that simple interpretation is not possible. In other CFQMC calculations, even for systems smaller than ours, assignment of the eigenstates was reported to be problematic. To our knowledge, only the parentage of the relaxed eigenvectors has been used to assign the character of eigenstates in CFQMC calculations. $H_5O_2^+$ is so complicated that often parentage is not sufficient for assignment. In this work, we calculated generalized transition moments

$$I_j^m = \langle \tilde{\phi}_0 | q_m | \tilde{\phi}_j \rangle \tag{29}$$

to facilitate the interpretation of excited states. In eq 29, $\tilde{\phi}_0$ and $\tilde{\phi}_j$ are ground and jth excited eigenfunctions, respectively, at a given projection time, and q_m is a coordinate operator that represents a specific vibrational motion and may not correspond to a physical dipole transition operator. The transition moments or any matrix elements of a scalar operator can be evaluated using the same random walks used in the estimation of the Hamiltonian and overlap matrixes, as suggested by Ceperley and Bernu.[52]

4.4. Specification of the Basis and Simulation Length. The excited basis functions are assembled as products of ψ_{trial} with the g_ν factors defined in Table 3. The N_p in eq 20 is limited to ≤ 2 so that only coupling between two modes is considered. The sum of $n_{\nu(i)}$ in a basis function f_i, $\sum_\nu n_{\nu(i)}$, is also ≤ 2 except for several low-energy modes that are mostly from the terminal water monomer wagging and torsion motions. For these low-frequency modes higher overtone basis functions are also included to make the basis set as complete as possible in this spectral range and prevent collapse of higher energy states to these overtones. For the rest of the modes such as bond stretch and bending modes, only vibrational fundamentals and the first overtone basis functions are selected as the excited basis set for the current study. A total of 131 basis functions with A_1^+ symmetry and 94 of B_1^+ symmetry were assembled in this manner.

An exhaustive variational calculation at zero projection time was performed with 40000 walkers for 100000 steps to construct the best initial trial wave functions. After the variational diagonalization, high-frequency states were omitted from the trial wave function set, only keeping the 90 lowest states in the A_1^+ block and 66 in the B_1^+ block as trial wave functions for the CFQMC run to reduce statistical noise and basis error. The CFQMC calculation was carried out with a large collection of 5720 independent walkers. Each walker has been propagated over 500000 steps. The time step used for this simulation was 1.0 in atomic units and the Hamiltonian and overlap matrix elements were evaluated at every 5 steps. For the quantitative estimation of converged eigenvalues, we performed a double-exponential fit to the eigenvalue curve to the limit of infinite projection time.

5. Results and Discussion

5.1. The Ground State. The energy of the ground vibrational state for the OSS3(p) potential is a number that we have determined precisely from diffusion and branching QMC calculations. Our best estimate of the ZPE is 12218.7($\pm$ 0.6) cm^{-1} extrapolated to zero QMC time step. An extrapolation to zero time step was not feasible in the current CFQMC calculations, which were run with a time step 1 au. Since the same imaginary time propagator is used in both the diffusion and breaching and CFQMC methods, we expect similar finite time step errors and expect CFQMC to yield a ground-state energy close to the diffusion and branching method at $\Delta t = 1$ au, which was 12222 cm^{-1} (see Figure 3 of ref 48).

We explored several ways of extracting eigenenergies from the CFQMC calculations. The most successful was diagonalization of the full Hamiltonian matrix in the projected basis, followed by extrapolation of the eigenvalues to infinite projection time. A plot of the ground state eigenvalue as a function of projection time is given in Figure 2a. Until a projection time of roughly 200 au the eigenvalue decays exponentially. Past 200 au growing statistical errors in the Hamiltonian matrix cause severe bias error of the apparent ground-state energy, and the lowest eigenvalue veers away from the true value. By a projection time of 350 au, the eigenvalue drops below the physical ZPE.

Until bias error overwhelms the calculation, exponential convergence to a true eigenvalue is expected as the imaginary time propagator eliminates high-lying contamination of the eigenstates. We found that a double-exponential fit to the time-dependent eigenvalue, accounting for the possibility of two major contaminants, was most successful at extrapolating the long time limit in a stable fashion. Figure 2b shows the ground-state energy extrapolated from data in Figure 2a as a function of the upper limit of the time range used in a double-exponential fit. Over a wide range of time, between upper limits of roughly 125$-$200 au, the extrapolated energy varied by <10 cm^{-1}. Since the ground state is more strongly affected by bias than other states, it is actually a difficult test case for the extrapolation of energy eigenvalues.

We explored a different route to derive eigenvalues from the CFQMC calculations. Bias error in the eigenvalues arises during diagonalization of a Hamiltonian subject to statistical noise. We observed that combinations of the form

$$\frac{H_{kk}(t)}{N_{kk}(t)} \tag{30}$$

often exhibited plateau behavior, indicating that projected state k was dominated by a single true eigenstate. Since diagonalization is not involved, estimation of an eigenvalue in this way is free of the most serious source of bias error. Of course, not all projected states show plateaus in $H_{kk}(t)/N_{kk}(t)$. We would always expect the true ground-state combination $H_{11}(t)/N_{11}(t)$ to exhibit plateau because there is no lower state to which it can collapse. Indeed, $H_{11}(t)/N_{11}(t)$ extrapolates to 12225 cm^{-1}, in agreement with our diffusion and branching QMC. This confirms that the CFQMC is properly relaxing the basis functions.

While eq 30 has the obvious advantage of freedom from bias error, it also has a drawback as an estimator of true eigenvalues. Contamination of eigenvalues from full diagonalization arise from basis functions that are not included anywhere in the projected basis. However, the estimator in eq 30 deviates from plateau behavior when projected state k is a true eigenfunction contaminated by any other eigenfunction, lying either within or outside the projected basis. As a consequence, the combination in eq 30, while having the desirable feature of not being susceptible to bias error collapse like that of the full diagonalization eigenvalue in Figure 2b, must be monitored for a rather long time before a reliable estimate of the eigenvalue is obtained. For example, $H_{11}(t)/N_{11}(t)$ up to a projection time of at least 400 au was required to accurately estimate the ZPE. On the

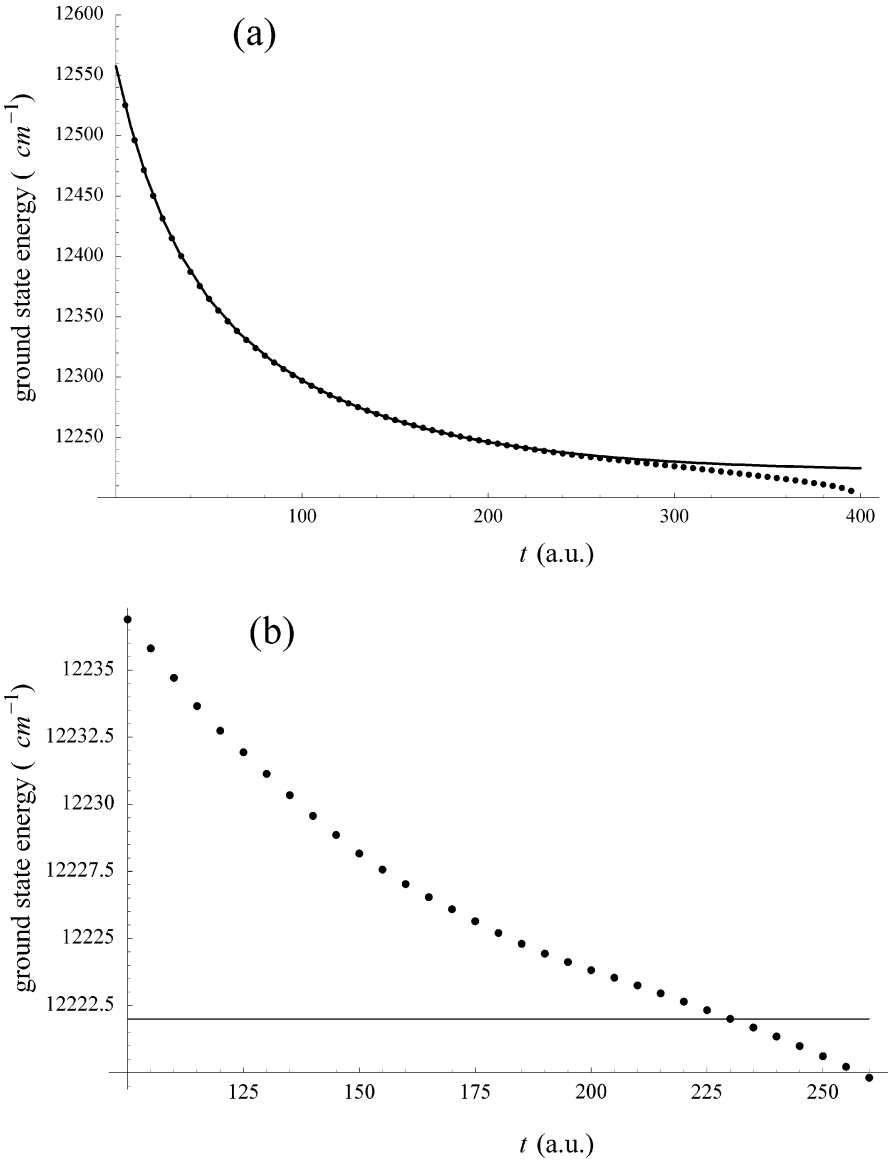

Figure 2. (a) The ground-state eigenvalue as a function of projection time *t*. (b) The extrapolated ground-state eigenvalue vs the upper limit of the time range used in a double-exponential fit.

other hand, full diagonalization results gave an accurate ZPE by about 125 au, and data beyond 200 au were severely compromised by bias error. Nevertheless, for excited states tracking the combination $H_{kk}(t)/N_{kk}(t)$ did prove useful in identifying stable, converged states in a crowded spectrum of excited states.

We also attempted to implement a minimum variance method that circumvents diagonalization as a method of finding eigenvalues because eigenvalues from diagonalization are subject to large bias error at the low and high end of the eigenvalue spectrum. We accumulated the expectation value of H^2 in the relaxed basis, $[H^2(t)]_{ij}$, and then sought states that minimized the variance $\langle H^2\rangle - \langle H\rangle^2$. As pointed out by Cerperley an Bernu, when eigenstates $\lambda_j(t)$ in eq 2 reach a plateau, the variance of the Hamiltonian operator vanishes. The *k*th state minimum variance is an eigenvector of the matrix,

$$2\langle E_k\rangle H_{ij} - H_{ij}^2 \tag{31}$$

where $\langle E_k\rangle$ is the energy expectation value $\mathbf{C}_k^t\mathbf{H}\mathbf{C}_k$. This is a nonlinear eigenvalue equation that has to be solved self-consistently. While states of minimum variance were far less susceptible to bias error than states that diagonalized the Hamiltonian, we were not able to accumulate $[H^2(t)]_{ij}$ with sufficient statistical accuracy to make this a feasible alternative to diagonalization of the Hamiltonian matrix.

5.2. The Excited States. Most of the fundamental vibrations of $H_5O_2^+$ could be identified from our CFQMC calculations using the generalized transition moments described in section 4.3. Generalized transition moments corresponding to motion of the central proton motion, oxygen−oxygen symmetric stretch, and wagging, bending, and stretching of the outer water units are presented in this section. Of these, motion of the central proton is expected to correspond with a strong physical transition moment. Some modes, like the oxygen−oxygen stretch, are IR inactive and have zero physical transition dipole associated with them. Assignment of the qualitative character of modes such as the oxygen−oxygen stretch is facilitated using the generalized transition moment [eq 29]. In this example, using the oxygen−oxygen stretch coordinate as q_m in eq 29 clearly identifies the eigenstate associated with this motion.

We were not able to extrapolate all excited state eigenvalues to infinite time like the ground state. Some of the projected states were strongly coupled to each other and their (imaginary)

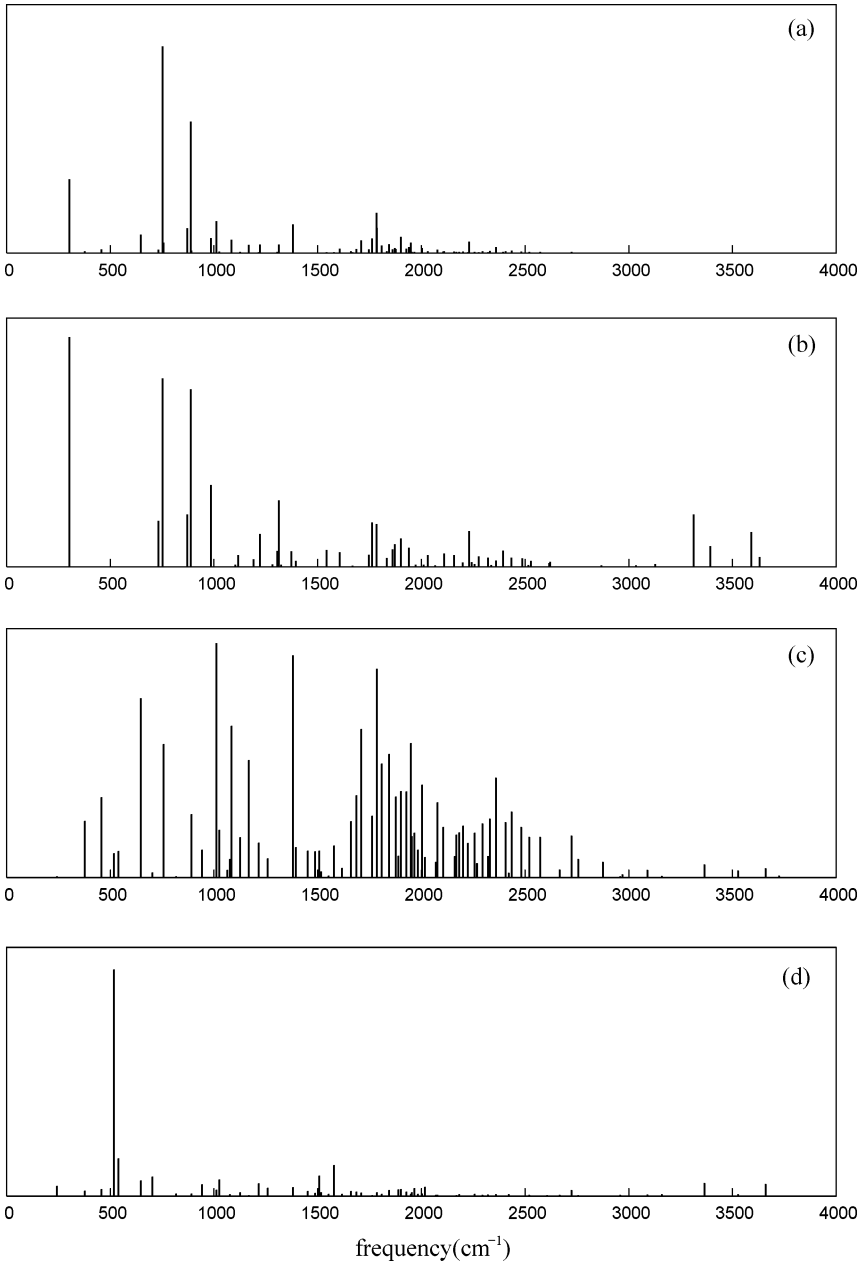

Figure 3. Transition moment intensity (in arbitrary units) for various motions of $H_5O_2^+$. The corresponding coordinates are given in the parentheses. (a) The central proton displacement (**r**[eq 21]). (b) The outer water wagging ($w_a - w_b$). (c) the Central proton bending (the *z*-component of **r**). (d) O···O stretch (*R*).

time evolution was more complex than could be captured with simple exponential fits. The appropriate fitting model for these states would be multistate fits with adjustable coupling, something we did not attempt in this work. However, when the coupling between crossing levels was weak, we were able to obtain smooth diabatic curves and perform reliable extrapolation.

We begin with a discussion of the modes associated with central proton motion. The total transition moment intensity, the square of all three components of the central proton vector [see eq 21] is shown in Figure 3a. A significant amount of central proton motion is associated with three eigenstates. Even previously calculated harmonic spectra for $H_5O_2^+$ show large intensity associated with more than one mode.[6] The transition moment intensity associated with only the *y*-component of central proton motion indicates that all of the three modes associated with the central proton involve motion of the proton along the oxygen−oxygen axis. The lowest energy central proton peak, least intense of the major central proton peaks, at 303 cm^{-1} in Figure 3a also shows up as the most intense peak in the transition moment spectrum of outer water wagging motion (Figure 3b). Hence, this peak is identified as the asymmetric proton transfer motion strongly coupled to wagging. The other two major central proton peaks in Figure 3a also exhibit considerable wagging intensity in Figure 3b. The middle peak in Figure 3a occurs at 737 cm^{-1}. It represents the transition with the highest contribution from proton-transfer motion. The other peak at 870 cm^{-1} is also mostly proton-transfer mode combined with mutual torsion motion of the two terminal water monomers.

We also searched for modes that would correspond to a central proton bend, that is, motion of the central proton perpendicular to the oxygen−oxygen vector. A candidate for a bending fundamental was visible near 1353 cm^{-1} in the transition moment spectrum for the *z*-component of the central

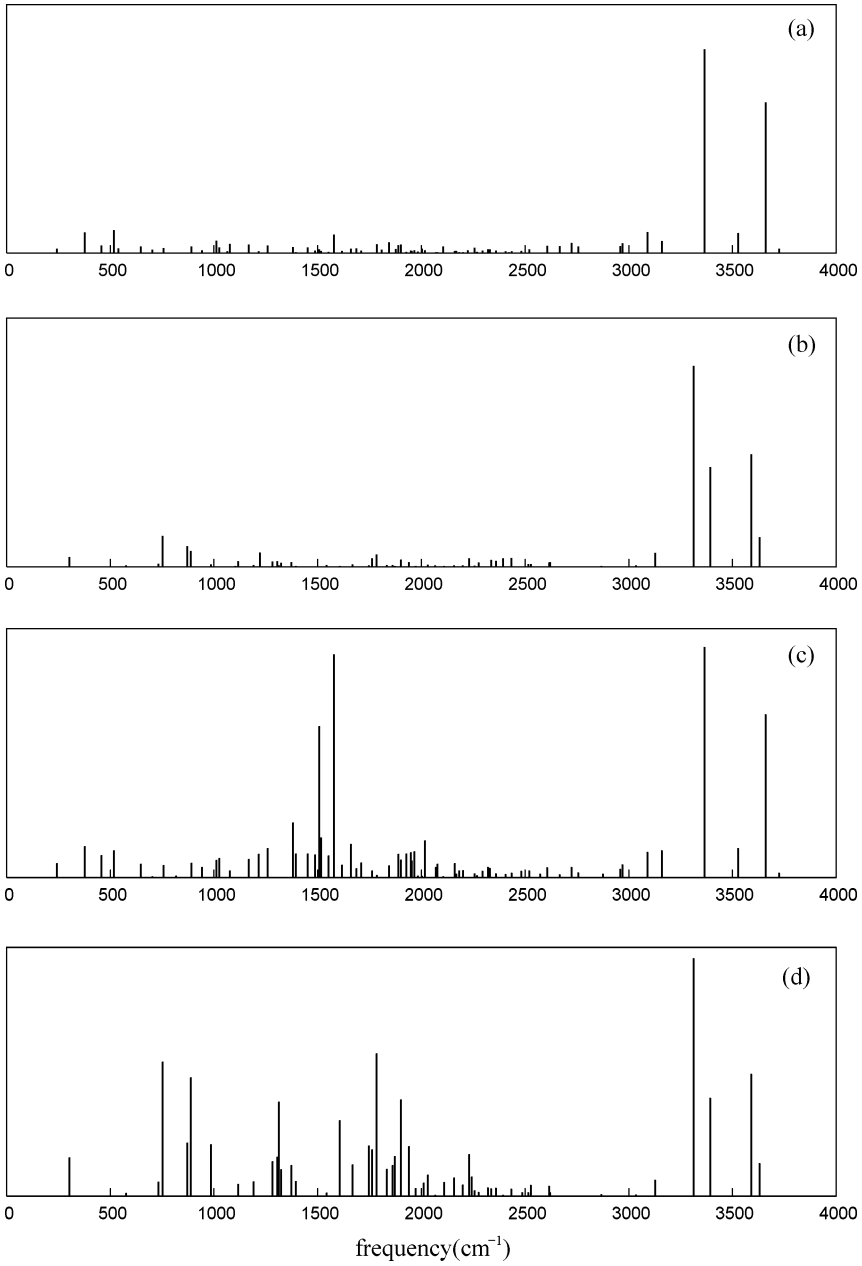

Figure 4. Transition moment intensity (in arbitrary units) for the motion of the outer waters. (a) Symmetric OH stretch. (b) Asymmetric OH stretch. (c) Symmetric outer water bending. (d) Asymmetric outer water bending.

proton (see Figure 3c). Unfortunately, none of the states with strong proton bending intensity were ones we could extrapolate reliably.

The modes with strong central proton intensity at 737 and 870 cm^{-1} in our calculations correspond to features observed by Asmis et al.[42] in recent infrared multiphoton photodissociation (IRMPD) experiments. A weak band centered at 788 cm^{-1} and strong features at 921, 1043, 1317, and 1741 cm^{-1} were observed in those experiments. Each of the strong bands contained several features, and it is not clear from the experiments what frequencies should be taken as the vibrational fundamentals. The ions in the experiment were estimated to be at a temperature of 100 K. Our peaks at 737 and 870 cm^{-1} might be candidates for assigning the experimental peaks at 788 and 921 cm^{-1} (for which the latter has a feature at 888 cm^{-1}). According to our generalized transition moment results, our peaks at 737 and 870 cm^{-1} both have O···H^+···O asymmetric stretch character and should have strong IR intensity. Dai et al.[49] identified only one mode as an O···H^+···O asymmetric stretch and suggested that it was associated with the 921 cm^{-1} feature in the IRMPD experiments. More experimental and theoretical work is required before conclusive assignments can be made.

The O···O stretch mode is a relatively pure mode in the CFQMC calculations with a small amount of mixing with the water wagging mode. It is well-resolved at 516 cm^{-1} without any confusion as seen in Figure 3d.

OH stretch modes of the outer water monomers are also of interest. Because these modes lie in a very high frequency region, by the nature of the CFQMC method it is more challenging to obtain reliable results. We could describe the symmetric OH stretch mode with A_1^+ symmetry without much trouble. Figure 4a shows the transition moment spectrum for this motion at 3375 cm^{-1}. The asymmetric OH stretch mode with B_1^+ symmetry proved difficult to obtain. We know that this mode exits near 3316 cm^{-1} as illustrated in Figure 4b and

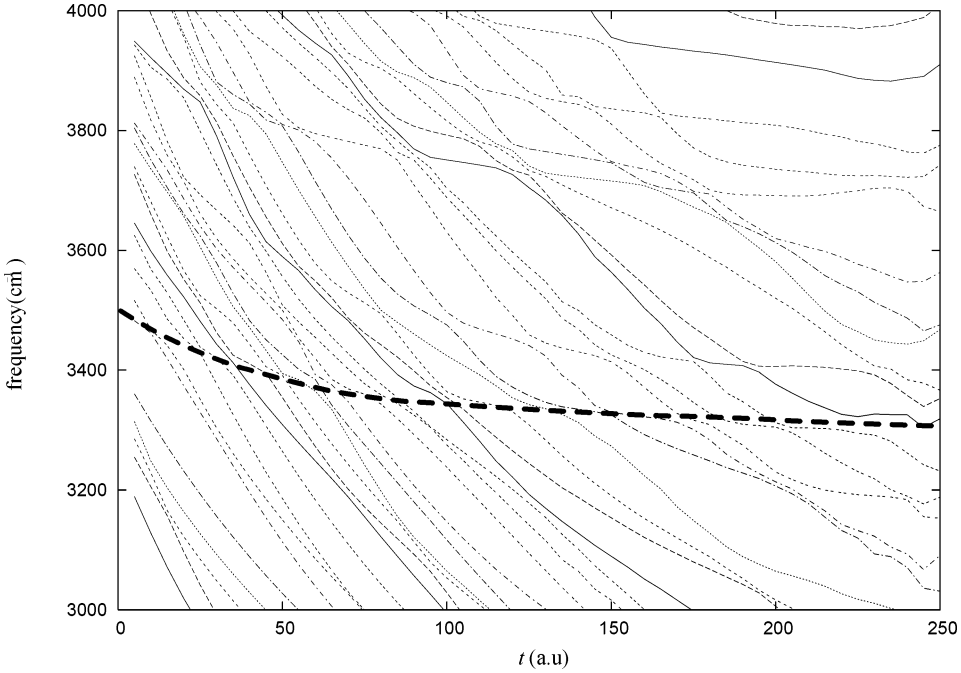

Figure 5. Eigenvalue spectrum near asymmetric OH stretch mode of the outer water monomers. A thick dashed curve just below 3400 cm^{-1} designates the corresponding state. Note that there are many crossings with other states.

Figure 5, but we were not able to extract a precise fit for this mode. The degenerate OH stretch mode with E^+ symmetry collapsed to lower energy E^+ states because of lack of basis functions of E^+ symmetry in our basis. The OH stretches are very strongly red-shifted by roughly 440 cm^{-1} from their harmonic frequencies. This indicates that the OH stretching modes are strongly coupled to other coordinates of $H_5O_2^+$. In fact, the VMC eigenstates at projection time zero show a large degree of mixing between OH stretch basis functions and many other coordinates. On the basis of the generalized transition moments displayed in Figure 4, we can identify the outer water bends as one of the coordinates coupling strongly with the OH stretches. The symmetric OH stretches and bends show common peaks in Figure 4a and Figure 4c, as do the corresponding asymmetric motions in Figure 4b and Figure 4d. The red shift of the OH stretches from their harmonic frequencies predicted by the OSS3(p) potential is too large. The experimental frequencies lie at 3609 cm^{-1} for symmetric stretch and 3684 cm^{-1} for asymmetric stretch.[39]

The water-bending transition moment intensity is given in Figure 4c and Figure 4d for each symmetry. The symmetric water-bending fundamental can be extracted from the CFQMC data and appears at 1583 cm^{-1}. The asymmetric water-bending mode is not as clear as the symmetric one as seen in Figure 4d. We assigned the peak at 1788 cm^{-1} as the asymmetric water-bending fundamental based on the relative intensity. Additional vibrational eigenenergies are given in Table 4 for which clear extrapolations were possible but for which assignments were problematic.

5.3. Discussion. In Table 4 we compared exact fundamental frequencies from the CFQMC calculations with the MULTIMODE results of Dai et al.[49] In all cases where we could make a firm comparison, the exact result was downshifted from the MULTIMODE frequency, typically 20−80 cm^{-1}. The O···O stretch, symmetric water bend, and symmetric outer water OH stretch are all firm comparisons where the assignment is clear and the CFQMC eigenvalues can be extrapolated to infinite time. The downshifts of the exact CFQMC eigenvalues from MULTIMODE results were 53, 73, and 45 cm^{-1}, respectively.

TABLE 4: Zero-Point Energy and Converged Excited Vibrational Frequencies of $H_5O_2^+$ in Wavenumbers[a]

vibrational energy			
CFQMC	15D VCI	sym.	assignment
12222(±1)	12320.6	A_1^+	ZPE
227(±2)		A_1^+	mutual torsion of outer waters
348 (±3)		A_1^+	water torsion
303(±1)	521	B_1^+	water wag
440(±2)		E^+	water torsion about bisectors
516(±4)	569	A_1^+	O···O stretch
737(±3)		B_1^+	O···H$^+$···O asym. stretch
870(±6)	902	B_1^+	O···H$^+$···O asym. stretch
1583	1656	A_1^+	sym. outer water bend
1788	1860	B_1^+	asym. outer water bend
3375	3420	A_1^+	sym. outer water OH stretch
813 (±4)		A_1^+	O···O stretch + mutual torsion of outer waters
1023(±4)		A_1^+	first overtone of O···O stretch
646(±4)		A_1^+	
1058(±4)		A_1^+	
572(±4)		B_1^+	
645(±9)		B_1^+	
1114(±12)		B_1^+	
1276		B_1^+	

[a] Vibrational frequencies are relative to the CFQMC zero-point energy of 12222 cm^{-1}. Miscellaneous vibrational frequencies for which we were not able to make a conclusive assignment are also reported. Corresponding 15D VCI results from ref 49 are listed for comparison. The statistical error estimated for selected CFQMC eigenvalues are standard deviations estimated by breaking the entire data set into four subsets and evaluating eigenvalues for each subset. This method supposes that the subset results behave as Gaussian random variables,[85] which is probably not accurate in some cases. However, it was not feasible to further divide the data sets and verify scaling of the variance with sample size. Other sources of error are discussed in section 5.3.

Evidently, the MULTIMODE program provides an excellent set of approximate eigenvalues for this very complex system, but the magnitude of these errors should be considered when

attempting a quantitative comparison with experiment. There are other cases in Table 4 where we listed corresponding CFQMC and MULTIMODE eigenvalues. In these cases comparison is not as firm for various reasons. For example, we found several modes with a significant O···H^+···O asymmetric stretch component, and it is not clear which one corresponds to the one identified by Dai et al. Furthermore, what is called a "wag" or "twist" may be open to interpretation, or the MULTIMODE and CFQMC eigenvectors may have a different nature.

The error estimate associated with the CFQMC eigenvalues in Table 4 is only one component of the possible error. It is the statistical error associated with variability in the results arising from a finite amount of statistical sampling. The error reported in Table 4 is calculated by breaking the total data set into 4 blocks and generating results for each of the blocks separately.[85] However, the statistical error is not the only source of error. (A useful discussion of the sources of error in CFQMC calculations can be found in ref 52.) Another source of error is the bias error, which arises because eigenvalues are a nonlinear function of the elements of N_{ij} and H_{ij} [eqs 13 and 14], and therefore averages of finite numbers of data points will systematically deviate from the true expectation value. We have designed our procedure for extracting vibrational eigenvalues from the data to minimize the effect of bias error. Specifically, the exponential fit is applied within a range of projection times in which the bias error is minimal. We have verified this by carefully checking the ground-state energy against our very accurate DMC value.[48] This is a stringent test because the ground state is highly susceptible to bias error: any error of the off-diagonal Hamiltonian matrix elements drives down the apparent ground-state energy.

The major source of error in our eigenvalue estimates is the extrapolation error. As discussed in sections 4.4 and 5.1, eigenvalues at infinite projection time are extracted by fitting the eigenvalues in a range of finite projection times to a sum of two exponentials. Figure 2 shows that the extrapolated energy of the ground state varies by $\sim$10 cm^{-1} over a wide variation in the range of projection times used in the fit. While this shows that the fitting procedure is robust, the variation of extrapolated eigenvalues is actually larger than the statistical error. On this basis, we conclude that the extrapolation error is the source of error that limits our results. Even though the statistical errors in Table 4 are quite small, the true errors should have an extra $\pm$7 cm^{-1} associated with the extrapolation.

6. Conclusions

The excited vibrational structure of the protonated water dimer was studied employing the CFQMC method to obtain information about the exact vibrational eigenvalues of the OSS3(p) potential. It should be noted that the problem is highly challenging because of the large number of strongly coupled degrees of freedom and very floppy nature of the system. Special attention was paid to the development of flexible basis functions, pre-optimized with variational Monte Carlo, and coordinates specifically designed for this system such as torsional coordinates of the outer water units. Given the flexibility, and hence complexity, of our trial basis, automated code generation techniques were used to implement the CFQMC calculation. Without these steps, obtaining converged results for this large, demanding molecule would not have been feasible. The calculated excited states are assigned by use of the transition moments, which turned out to be a useful tool to analyze the complex eigenvalue spectrum. The central proton motion, oxygen−oxygen symmetric stretch, and wagging, bending, and stretching of the outer water units were successfully resolved. As for the central proton transfer mode, we found three intense peaks associated with asymmetric proton stretch motion. We also found that low-energy eigenstates mostly due to the outer water torsion and wagging motion were coupled with proton stretch mode. Comparing with the experimental spectrum, the fundamental frequency of the OH stretch modes of the outer water monomers were underestimated significantly by the OSS3-(p) surface. The experimental frequencies lie at 3609 cm^{-1} for the symmetric stretch and 3684 cm^{-1} for the asymmetric stretch, downshifted from harmonic frequencies of 3796 and 3700 cm^{-1}, respectively. The OSS3(p) surface overestimates the harmonic frequencies of the OH stretches and underestimates the fundamentals when coupled to the rest of the molecules. The OSS3-(p) surface should be more accurate for the low-frequency, large-amplitude modes where greater attention was focused in the design of the surface.

To understand the complex vibrational motion of the $H_5O_2^+$ molecular ion, improved potential surfaces need to be developed and vibrational eigenvalues computed for comparison with experiment. This work demonstrates that CFQMC methods can provide useful benchmarks to assist these developments.

Acknowledgment. We acknowledge NSF Grant No. CHE-0109243 for supporting this work and the Ohio Supercomputer Center for resources needed to perform the calculations reported here. This paper is presented to honor Gert Billing's many significant contributions to the field of chemical dynamics.

References and Notes

(1) Kebarle, P.; Searles, S. K.; Zolla, A.; Scarborough, J.; Arshadi, M. *J. Am. Chem. Soc.* **1967**, *89* (25), 6393.
(2) Cunningham, A. J.; Payzant, J. D.; Kebarle, P. *J. Am. Chem. Soc.* **1972**, *94* (22), 7627.
(3) Meot-Ner, M.; Field, F. H. *J. Am. Chem. Soc.* **1977**, *99* (4), 998.
(4) Lau, Y. K.; Ikuta, S.; Kebarle, P. *J. Am. Chem. Soc.* **1982**, *104* (6), 1462.
(5) Magnera, T. F.; David, D. E.; Michl, J. *Chem. Phys. Lett.* **1991**, *182*, 363.
(6) Ojamäe, L.; Shavitt, I.; Singer, S. J. *Int. J. Quantum Chem., Quantum Chem. Symp.* **1995**, *29*, 657.
(7) Yamabe, S.; Minato, T.; Hirao, K. *J. Chem. Phys.* **1984**, *80* (4), 1576.
(8) Frisch, M. J.; Del Bene, J. E.; Binkley, J. S.; Schaefer, H. F., III. *J. Chem. Phys.* **1986**, *84* (4), 2279.
(9) Lee, E. F.; Dyke, J. M. *Mol. Phys.* **1991**, *73*, 375.
(10) Xie, Y.; Remington, R. B.; Schaefer, H. F., III. *J. Chem. Phys.* **1994**, *101* (6), 4878.
(11) Pudzianowski, A. T. *J. Chem. Phys.* **1995**, *102* (19), 7761.
(12) Tuma, C.; Boese, A. D.; Handy, N. C. *Phys. Chem. Chem. Phys.* **1999**, *1* (17), 3939.
(13) Newton, M. D.; Ehrenson, S. *J. Am. Chem. Soc.* **1971**, *93*, 4971.
(14) Olovsson, I. *J. Chem. Phys.* **1968**, *49* (3), 1063.
(15) Wales, D. J. *J. Chem. Phys.* **1999**, *110* (21), 10403.
(16) Valeev, E. F.; Schaefer, H. F., III. *J. Chem. Phys.* **1998**, *108* (17), 7197.
(17) Wei, D.; Salahub, D. R. *J. Chem. Phys.* **1994**, *101* (9), 7633.
(18) Mijoule, C. *Chem. Phys. Lett.* **1993**, *208*, 364.
(19) Barone, V.; Orlandini, L.; Adamo, C. *Chem. Phys. Lett.* **1994**, *231*, 295.
(20) Liao, H.-Y.; Chu, S.-Y. *Int. J. Quantum Chem.* **2002**, *90*, 507.
(21) Auer, A. A.; Helgaker, T.; Klopper, W. *Phys. Chem. Chem. Phys.* **2000**, *2* (10), 2235.
(22) Salvador, P.; Duran, M.; Dannenberg, J. J. *J. Phys. Chem. A* **2002**, *106* (29), 6883.
(23) Scuseria, G. E.; Scheiner, A. C.; Lee, T. J.; Rice, J. E.; Schaefer, H. F., III. *J. Chem. Phys.* **1986**, *86* (5), 2881.
(24) Muguet, F. F. *J. Mol. Struct. (THEOCHEM)* **1996**, *368*, 173.
(25) Klein, S.; Kochanski, E.; Strich, A.; Sadlej, A. J. *J. Phys. Chem. A* **1997**, *101* (26), 4799.
(26) Williams, G. R. J. *J. Mol. Struct. (THEOCHEM)* **1986**, *138*, 333.
(27) Kollman, P. A.; Allen, L. C. *J. Am. Chem. Soc.* **1970**, *92*, 6101.
(28) Zundel, G.; Frish, M. J. In *The Chemical Physics of Solvation*; Dogonadze, R., K'alm'an, E., Kornyshev, A. A., Ulstrup, J., Eds.; Elsevier: Amsterdam, 1986; Vol. 2, Chapter 2.

(29) Essayem, N.; Holmqvist, A.; Vedrine, P. Y. G. J. C.; Taarit, Y. B. *J. Catal.* **2001**, *197*, 273.
(30) Yukhnevich, G. V.; Tarakanova, E. G.; Mayorov, V. D.; Librovich, N. B. *J. Mol. Struct.* **1992**, *265*, 237.
(31) Sato, S.; Ido, A.; Ishida, H. *J. Chem. Phys.* **2000**, *113* (17), 7453.
(32) Jones, D. J.; Roziere, J.; Penfold, J.; Tomkinson, J. *J. Mol. Struct.* **1989**, *195*, 283.
(33) Librovich, N. B.; Maiorov, V. D. *Dokl. Akad. Nauk SSSR* **1975**, *225*, 1358.
(34) Librovich, N. B.; Sakun, V. P.; Sokolov, N. D. *Chem. Phys.* **1979**, *39*, 351.
(35) Librovich, N. B.; Sakun, V. P.; Sokolov, N. D. *Chem. Phys.* **1981**, *60*, 425.
(36) Vener, M. V.; Sauer, J. *Chem. Phys. Lett.* **1999**, *312* (5, 6), 591.
(37) Vener, M. V.; Kühn, O.; Sauer, J. *J. Chem. Phys.* **2001**, *114*, 240.
(38) Zygmunt, S. A.; Curtiss, L. A.; Iton, L. E. *J. Phys. Chem. B* **2001**, *105* (15), 3034.
(39) Yeh, L.; Okumura, M.; Myers, J.; Price, J.; Lee, Y. *J. Chem. Phys.* **1989**, *91* (12), 7319.
(40) Okumura, M.; Yeh, L.; Myers, J.; Lee, Y. T. *J. Phys. Chem.* **1990**, *94* (9), 3416.
(41) Yeh, L.; Lee, Y.; Hougen, J. *J. Mol. Spectrosc.* **1994**, *164* (2), 473.
(42) Asmis, K. R.; Pivonka, N. L.; Santambrogio, G.; Brümmer, M.; Kaposta, C.; Neumark, D. M.; Wöste, L. *Science* **2003**, *299* (5611), 1375.
(43) Termath, V.; Sauer, J. *Mol. Phys.* **1997**, *91*, 963.
(44) Wei, D.; Salahub, D. R. *J. Chem. Phys.* **1997**, *106* (14), 6086.
(45) Cheng, H.-P.; Krause, J. L. *J. Chem. Phys.* **1997**, *107* (20), 8461.
(46) Sagnella, D. E.; Tuckerman, M. E. *J. Chem. Phys.* **1998**, *108* (5), 2073.
(47) Chaban, G. M.; Jung, J. O.; Gerber, R. B. *J. Phys. Chem. A* **2000**, *104* (12), 2772.
(48) Huang, X.; Cho, H. M.; Carter, S.; Ojamäe, L.; Bowman, J. M.; Singer, S. J. *J. Phys. Chem. A* **2003**, *107* (37), 7142.
(49) Dai, J.; Bačić, Z.; Huang, X.; Carter, S.; Bowman, J. M. *J. Chem. Phys.* **2003**, *119* (13), 6571.
(50) Lobaugh, J.; Voth, G. A. *J. Chem. Phys.* **1996**, *104*, 2056.
(51) Pavese, M.; Chawla, S.; Lu, D.; Lobaugh, J.; Voth, G. A. *J. Chem. Phys.* **1997**, *107* (18), 7428.
(52) Ceperley, D. M.; Bernu, B. *J. Chem. Phys.* **1988**, *89* (10), 6316.
(53) Acioli, P. H.; Soares Neto, J. J. *J. Mol. Struct. (THEOCHEM)* **1999**, *464*, 145.
(54) Brown, W. R.; nad W. A. Lester, W. A. G., Jr. *J. Chem. Phys.* **1995**, *103* (22), 9721.
(55) Acioli, P.; Costa, L. S.; Prudent, F. V. *Chem. Phys. Lett.* **2000**, *321*, 121.
(56) Acioli, P. H.; Costa, L. S.; Prudent, F. V. *J. Chem. Phys.* **1999**, *111* (14), 6311.
(57) Prudent, F. V.; Acioli, P. *Chem. Phys. Lett.* **1999**, *302*, 249.
(58) Costa, L. S.; Prudent, F. V.; Acioli, P. *Phys. Rev. A* **2000**, *61* (1), 012506.
(59) Nightingale, M. P.; Blöte, H. M. J. *Phys. Rev. Lett.* **1998**, *80* (5), 1007.
(60) Nightingale, M. P.; Blöte, H. M. J. *Physica A* **1998**, *251*, 211.
(61) Nightingale, M. P.; Umrigar, C. J. *Adv. Chem. Phys.* **1999**, *105*, 65.
(62) Jones, M. D.; Ortiz, G.; Ceperley, D. M. *Phys. Rev. E* **1997**, *55* (5), 6202.
(63) Prudent, F. V.; Costa, L. S.; Acioli, P. H. *J. Phys. B: At. Mol. Opt. Phys.* **2000**, *33*, R285.
(64) Jarrell, M.; Gubernatis, J. E. *Phys. Rep.* **269**, *269*, 133.
(65) Caffarel, M.; Claverie, P. *J. Chem. Phys.* **1988**, *88* (2), 1088.
(66) Caffarel, M.; Claverie, P. *J. Chem. Phys.* **1988**, *88* (2), 1100.
(67) Blume, D.; Lewerenz, M.; Whaley, K. B. *J. Chem. Phys.* **1997**, *107* (21), 9067.
(68) Blume, D.; Lewerenz, M.; Niyaz, P.; Whaley, K. B. *Phys. Rev.* **1997**, *E55* (3), 3664.
(69) Blume, D.; Lewerenz, M.; Whaley, K. B. *Math. Comput. Simul.* **1998**, *47* (2−5), 133.
(70) Blume, D.; Mladenovic, M.; Lewerenz, M.; Whaley, K. B. *J. Chem. Phys.* **1999**, *110* (12), 5789.
(71) Huang, P.; Viel, A.; Whaley, K. B. In *Recent Advances in Computational Chemistry*, Vol. 2, part 2; World Scientific: River Edge, NJ, 2002; p 111.
(72) Anderson, J. B. *J. Chem. Phys.* **1976**, *65* (10), 4121.
(73) Suhm, M. A.; Watts, R. O. *Phys. Rep.* **1991**, *204* (4), 293.
(74) Quack, M.; Suhm, M. A. *J. Chem. Phys.* **1991**, *95* (1), 28.
(75) Kuhn, B.; Rizzo, T. R.; Luckhaus, D.; Quack, M.; Suhm, M. A. *J. Chem. Phys.* **1999**, *111* (6), 2565.
(76) Caffarel, M.; Claverie, P.;.; Mijoule, C.; Andzelm, J.; Salahub, D. R. *J. Chem. Phys.* **1989**, *90* (2), 990.
(77) Sandler, P.; Buch, V.; Sadlej, J. *J. Chem. Phys.* **1996**, *105* (23), 10387.
(78) Lee, H.-S.; Herbert, J. M.; McCoy, A. B. *J. Chem. Phys.* **1999**, *110* (12), 5481.
(79) Lee, H.-S.; Herbert, J. M.; McCoy, A. B. *J. Chem. Phys.* **1999**, *111* (20), 9203.
(80) Severson, M. W.; Buch, V. *J. Chem. Phys.* **1999**, *111* (24), 10866.
(81) Bernu, B.; Ceperley, D. M.; Lester, W. A., Jr. *J. Chem. Phys.* **1990**, *93* (1), 552.
(82) da Silva, W. B.; Acioli, P. H. *J. Chem. Phys.* **2001**, *114* (22), 9720.
(83) Morse, P. M. *Phys. Rev.* **1929**, *34* (1), 57.
(84) Mathematica, Wolfram Research, Inc.: Champaign, IL, 1999.
(85) Flyvbjerg, H.; Petersen, H. G. *J. Chem. Phys.* **1989**, *91* (1), 461.